Upper limit on the gas density in the β Pictoris system

Thébault, P.; Augereau, J.-C.

A&A 437, 141–148 (2005)
DOI: 10.1051/0004-6361:20042594

Astronomy & Astrophysics

Upper limit on the gas density in the β Pictoris system

The effect of gas drag on dust dynamics

P. Thébault[1,2] and J.-C. Augereau[3,4]

[1] Stockholm Observatory, Albanova Universitetcentrum, 10691 Stockholm, Sweden
e-mail: philippe.thebault@obspm.fr
[2] Observatoire de Paris, Section de Meudon, 92195 Meudon Principal Cedex, France
[3] Leiden Observatory, PO Box 9513, 2300 RA Leiden, The Netherlands
[4] Laboratoire d'Astrophysique de l'Observatoire de Grenoble, BP 53, 38041 Grenoble Cedex 9, France

Received 22 December 2004 / Accepted 16 February 2005

Abstract. We investigate the effect of gas drag on the dynamics of the dust particles in the edge-on β Pictoris disc to derive an upper limit on the mass of gas in this system. Our study is motivated by the large uncertainties on the amount of gas in the β Pictoris disc currently found in the literature. The dust particles are assumed to originate from a colliding annulus of planetesimals peaking around 100 AU from the central star. We consider the various gas densities that have been inferred from independent observing techniques and we discuss their impact on dust dynamics and on the disc profile in scattered light along the midplane. We show that the observed scattered light profile of the disc cannot be properly reproduced if the hygrogen gas number density at 117 AU exceeds 10^4 cm^{-3}. This corresponds to an upper limit on the total gas mass of about 0.4 $M_\oplus$ and thus to a gas to dust mass ratio smaller than 1. Our approach therefore provides an independent diagnostic of gas depletion in the β Pictoris system relative to the dust disc. Such an approach could also be used to constrain the gas content of recently identified systems like the edge-on disc around AU Mic.

Key words. stars: planetary systems – stars: individual: β Pictoris– planetary systems: protoplanetary disks – planets and satellites: formation

1. Introduction

The β Pictoris system is one of the best-known examples of a debris disc surrounding a young Main Sequence star. The dust component of the almost edge-on disc has been thoroughly observationally investigated, in thermal emission as well as in scattered light (e.g. Artymowicz 1997, and references therein). The total dust mass is believed to range between a few lunar masses and 0.5 $M_\oplus$ (e.g. Zuckerman & Becklin 1993; Artymowicz 1997; Dent et al. 2000). These estimates lead to collisional lifetimes of dust particles which are much shorter than the estimated age of the system (8–20 Myr, Zuckerman et al. 2001; Song et al. 2003; Di Folco et al. 2004), which implies that the dust disc cannot be primordial but has to be replenished by collisions or evaporation of larger bodies (e.g. Artymowicz 1997; Lecavelier et al. 1996). Scattered light midplane surface brightness profiles display a sharp decrease beyond 120 AU (Kalas & Jewitt 1995) where the luminosity profile follows a steep radial power law r^α with $-5.5 < \alpha < -4.5$ (Heap et al. 2000). These outer regions of the disc that extend over hundreds of AU are believed to be made of small grains primarily produced within 150 AU and placed on high eccentricity orbits by radiation pressure (Lecavelier et al. 1996; Augereau et al. 2001).

In contrast to our relatively good knowledge of the dust distribution, the gaseous compound is still poorly constrained. This is in particular the case for hydrogen, which should a priori make up most of the gas disc. So far, attempts to directly detect hydrogen have failed, with the exception of the ISO observations by Thi et al. (2001) who have measured H_2 infrared emission features associated with pure rotational transitions. The mid-infrared observations are consistent with more than 50 $M_\oplus$ of warm H_2 in the β Pictoris disc. These results are challenged by the non-detection in the UV with the FUSE satellite of absorption lines from the H_2 electronic transition (Lecavelier et al. 2001). This non-detection places an upper limit on the H_2 column density three orders of magnitude smaller than the value derived from the infrared observations.

The H_2 emission is unlikely to be of interstellar origin according to Lecavelier et al. (1996). The ISO aperture being large, the infrared emission could originate from regions not probed by FUSE if the gas disc is very spatially extended. Recent mid-infrared observations with Spitzer nevertheless do not confirm the 17.035 μm H_2 emission feature observed with

ISO (Chen et al. 2004). The gas mass upper limit based on the Spitzer results is 11 $M_\oplus$, assuming a gas temperature of 110 K.

Attempts have also been made to indirectly reconstruct the hydrogen abundance from other more accurately observed species. Absorption lines in the stellar spectrum have indeed revealed the presence of numerous metallic elements (e.g. Hobbs et al. 1985; Lagrange et al. 1998; Roberge et al. 2000). From early estimates, rescaling to solar abundances led to column densities of $N(\mathrm{H}) = 10^{18}$–4×10^{20} cm^{-2} (Hobbs et al. 1985). Kamp et al. (2003) performed emission line calculations for different gas tracers (CO but also C and C$^+$) in the disc. They conclude that the total β Pictoris gas mass (presumably mostly made of hydrogen) would lie between 0.2 and 4 $M_\oplus$. More recently, Brandeker et al. (2004), using the VLT/UVES instrument, spatially resolved the gas disc and observed numerous emission lines, mainly from FeI and CaII, as well as NaI that was observed as far as 323 AU from the star. Estimating an ionisation structure for the disc and assuming solar abundances, they found a column density for atomic hydrogen of $N(\mathrm{HI}) = 8 \times 10^{18}$ cm^{-2}, consistent with the upper limit of Freudling et al. (1995), and $N(\mathrm{H_2}) = 3 \times 10^{18}$ cm^{-2} for molecular hydrogen, consistent with the Lecavelier et al. (2001) upper limit. However, the inferred total mass of the gas disc, $\simeq$0.1 $M_\oplus$, is inconsistent with the 50 $M_\oplus$ gas mass measured with ISO by Thi et al. (2001).

Nevertheless, independent considerations might argue in favour of a more massive gas disc. One puzzling result deduced from the observed absorption lines is that all ion species seem to be on Keplerian orbits, with low relative radial velocities (Olofsson et al. 2001). This is in strong contradiction to the fact that many of these elements should be rapidly ejected on unbound orbits by strong stellar radiation pressure (β Pictoris is an A5V star). Several explanations have been proposed to explain this contradiction. One of them is that gaseous friction due to an unseen gaseous braking agent, possibly hydrogen, should damp the outward outflow (Liseau 2003). With calculations based on the Liseau et al. (1999) model, Brandeker et al. (2004) estimated that a high density gas disc of $\simeq$50 $M_\oplus$ could lead to radial velocities compatible with the observed ones provided the disc is metal-depleted.

There are thus still large uncertainties regarding the amount of gas in the β Pictoris disc. We propose here to address this issue by looking at the effect of gaseous friction on the dynamics of the dust grains observed in scattered light. This approach is used to constrain the gas density in the disc and its radial distribution. We base our approach on the results of Augereau et al. (2001), who have shown that the observed dust disc could be successfully modeled if the grains are produced by a distribution of parent bodies within 150 AU from the central star and placed on orbits with large semi-major axis (a) and high eccentricities (e) by radiation pressure. The important point is that this satisfying fit of the surface brightness profile was obtained for a *gas-free* system.

Our main goal here is to estimate how gas drag might affect these results, and in particular which gas disc densities and distributions yield dust density profiles still compatible with observations and which ones do not and might thus be ruled out. Our approach is in the spirit of the remarkable pioneering work of Lecavelier et al. (1996), who explored the scattered light profile for different parent body prescriptions and even included gas drag, but considered a formal gas disc prescription ($\rho_g \propto 1/r$) and restricted their approach to $\beta < 1$ particles (note that the behaviour of $\beta > 1$ particles was addressed by Lecavelier et al. (1998) in the case of BD+31643, a very different stellar environment). This neglect of the $\beta > 1$ particles might be too restrictive in the presence of efficient gas drag which prevents high β particles from leaving the system as quickly as in a gas-free disc (see Sect. 2.2 and Fig. 2). Furthermore, at that time the radial power law index for the outer midplane luminosity profile was believed to be in the $[-3.6, -4.3]$ range rather than in the $[-4.5, -5.5]$ range.

2. Model

2.1. Equations of motion

Our integrator is a classic 4th order Runge-Kutta that test runs (performing mutual comparisons with higher order algorithms) have proved to be of satisfying accuracy for the present study. The integrator takes into account the star's central potential, the radiation pressure force and gaseous friction. The radiation pressure on a grain of mass m at a distance r from the central star is expressed as a function of the gravitational potential through the usual β parameter

$$\boldsymbol{F}_{\mathrm{rad}} = -\beta \boldsymbol{F}_{\mathrm{grav}} = \beta \frac{GMm}{r^2} \boldsymbol{r}, \tag{1}$$

assuming an optically thin disc in all directions. Here G is the gravitational constant and M the mass of the central star. We will consider grains larger than 0.1 μm radius, for which there is an inverse one to one relation between β and grain size s (Artymowicz 1988) and we assume $\beta \simeq 0.5 \times (5\ \mu\mathrm{m}/s)$ with s expressed in μm. For the gas drag force we follow Takeuchi & Artymowicz (2001) and adopt the Kwok (1975) formalism

$$\boldsymbol{F}_{\mathrm{gas}} = -\pi \rho_{\mathrm{g}}\, s^2 \left(v_{\mathrm{T}}^2 + \Delta v^2\right)^{1/2} \boldsymbol{\Delta v} \tag{2}$$

where ρ_{g} is the gas density, v_{T} is the gas thermal velocity and Δv is the difference between the grain velocity v and the gas velocity v_{g} expressed as a function of the Keplerian velocity v_{k}

$$v_{\mathrm{g}} = v_{\mathrm{K}}(1 - \nu)^2. \tag{3}$$

The parameter ν depends on the gas pressure gradient $\mathrm{d}P_{\mathrm{g}}/\mathrm{d}r$ and is

$$\nu = \frac{1}{r\Omega^2 \rho_{\mathrm{g}}} \frac{\mathrm{d}P_{\mathrm{g}}}{\mathrm{d}r}. \tag{4}$$

2.2. Dust disc

We assume that the dust particles are produced by parent bodies on circular orbits following the distribution derived by Augereau et al. (2001) and displayed in Fig. 1. This parent body distribution has been shown to produce a spatially extended dust disc that correctly matches the resolved scattered light images as well as the long-wavelength photometric data. The parent body distribution also results in a simulated disc radial

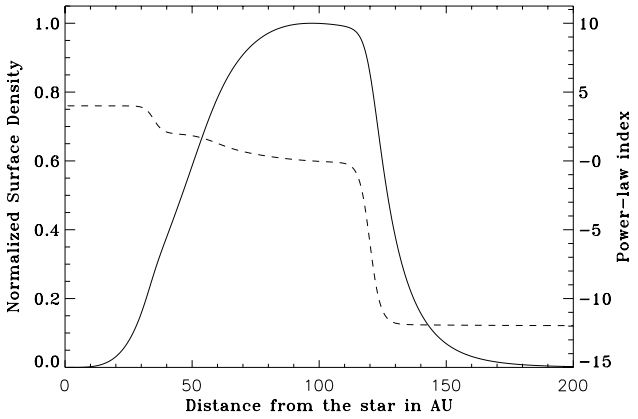

Fig. 1. Surface density of the parent bodies disc responsible for the resolved scattered light images according to Augereau et al. (2001, solid line). The dashed line together with the right y axis give the power-law index of the profile.

brightness profile at 12 μm consistent with the N-band thermal images obtained by Pantin et al. (1997) beyond ~30 AU. Importantly, Augereau et al. (2001) could not reproduce the absolute flux that they attribute to an additional population of very small grains with β ratios likely larger than 0.5. Recent mid-infrared observations support this picture (Okamoto et al. 2004; Telesco et al. 2005). The adopted distribution of parent bodies displayed in Fig. 1 peaks in the 80–120 AU region and cuts off beyond 150 AU (for the validity of this assumption in the context of the present paper see discussion in Sect. 4).

The differential size distribution of the dust produced is assumed to follow the usual equilibrium power law $\mathrm{d}N = C_0 s^{-3.5}\mathrm{d}s$ (Dohnanyi 1969). We then consider an arbitrary number of particles $N_{\rm num}$ satisfying this distribution between $s_{\rm min} = 0.1$ μm ($\beta = 25$) and $s_{\rm max} = 500$ μm ($\beta = 0.005$). We consider objects up to high β because gas drag might be very efficient in slowing down the escape of these small grains, hence increasing their contribution to the luminosity profile (for a more quantitative analysis, see Sect. 3). In order to get statistical significance for all size ranges despite the steep power law of the size distribution, three different runs, each with $N_{\rm num} = 20\,000$, are performed for the $0.005 < \beta < 0.05$, $0.05 < \beta < 0.5$ and $0.5 < \beta < 25$ populations, which are then recombined with the appropriate weights.

At each moment each particle is assigned a collision destruction probability, depending on its size, velocity and location in the disc, and has thus a limited lifetime. Due to obvious computational constraints, a realistic modeling of collisions is excluded here. We use an empirical approach where each particle is assigned, at each timestep, a collisional destruction probability depending on its β value, its distance r from the central star and its radial velocity v_r

$$f_{\rm coll} = \frac{\Delta t}{t_{\rm coll}} \tag{5}$$

where Δt is the simulation timestep and $t_{\rm coll}$ the collision time scale. We approximate $t_{\rm coll}$ by

$$t_{\rm coll} = \left(\frac{\beta_0}{\beta}\right)^{\alpha} \left(\frac{n_{100\,\rm AU}}{n_r}\right) \left(\frac{r}{100\,\rm AU}\right)^{0.5} \frac{v_{r_0}}{v_r}\, t_{\rm coll_0} \tag{6}$$

where $t_{\rm coll_0} \simeq 10^4$ years is a reference collision timescale that we take equal to the estimate of Artymowicz (1997) for a $\beta_0 = 0.3$ particle at 100 AU from the central star. v_{r_0} is the radial velocity of the β_0 particles at 100 AU and n_r is the volumic number dust density at distance r. The β (i.e. grain size) dependency of $t_{\rm coll}$ relies on complex physical parameters. However, numerical studies (e.g. Fig. 7 of Wyatt & Dent (2002) and Fig. 12 of Thébault et al. 2003) indicate that the coefficient α ranges between 0.3 and 0.5 for small particles. We here take $\alpha = 0.4$. The absolute value of the collision rates might be rescaled by changing the $t_{\rm coll_0}$ parameter.

For n_r in Eq. (6) we assume the dust density profile derived by Augereau et al. (2001) (see their Fig. 2) from the parent body profile displayed in Fig. 1. A more coherent approach would have consisted of taking into account, for each individual simulation, an n_r matching the final dust distribution. But this would have added much complexity to the problem by introducing a circular argument, the final distribution being in principle dependent on the assumed collision timescale. We nevertheless empirically checked the validity of our prescription by performing one test run with n_r matching the final dust distribution obtained in the reference case of Sect. 3.1, and ended up with a final luminosity profile which never departs by more than 10% from the nominal one. Possible errors due to the inevitable departure between the assumed n_r prescription and the final dust distribution are thus expected to be negligible compared to the impact of the parameters explored throughout the paper on the calculated brightness profiles.

Such an empirical prescription is only a crude approximation of the real collisional behaviour of dust particles. To the first order, it nevertheless provides a good indication of how the collision rate relies on the grain size, on the grain velocity and position in the disc[1].

2.3. Gas disc characteristics

Several test gas discs, with different profiles and spatial extents, are explored. Our reference case is the profile derived by Brandeker et al. (2004) from their observations of metallic emission lines, in particular NaI, out to 323 AU. From the observed NaI profile they deduced the radial density profile of hydrogen nuclei to be

$$n(\mathrm{H}) = n_0 \left[\left(\frac{r}{r_0}\right)^{2.4} + \left(\frac{r}{r_0}\right)^{5.3}\right]^{-\frac{1}{2}} \mathrm{cm}^{-3} \tag{7}$$

with $r_0 = 117$ AU.

We will explore different n_0 values between the two extreme values considered by Brandeker et al. (2004):

1. $n_0 = 2.25 \times 10^3$ cm^{-3}, required if solar abundances are assumed, which leads to a total H mass of $\simeq 0.1\ M_\oplus$,
2. a much higher density: $n_0 = 10^6$ cm^{-3} that implies a significant departure from solar abundances but is required, according to Brandeker et al. (2004), if hydrogen is to act

[1] a similar, although simpler, cut-off lifetime prescription acting as a substitute for collisional dust dectruction has been used recently by Deller & Maddison (2005).

Table 1. Summary of the different gas disc properties assumed in this paper. The densities n_0 are given at a distance r_0 = 117 AU from the star.

	n_0 [cm^{-3}]	Radial profile	Total mass [$M_\oplus$]	Comment
case 1	10^6	Brandeker et al. (2004)	40 $M_\oplus$	density required for the "gaseous braking agent" hypothesis
case 2	2.25×10^3	Brandeker et al. (2004)	0.1 $M_\oplus$	reconstructed from the NaI profile assuming solar abundances
case 3	10^4	Brandeker et al. (2004)	0.4 $M_\oplus$	
case 4	10^5	Brandeker et al. (2004)	4 $M_\oplus$	
case 5	10^6	Brandeker et al. (2004)	15 $M_\oplus$	truncated at 150 AU
case 6	7×10^5	Hayashi ($r^{-2.75}$)	40 $M_\oplus$	

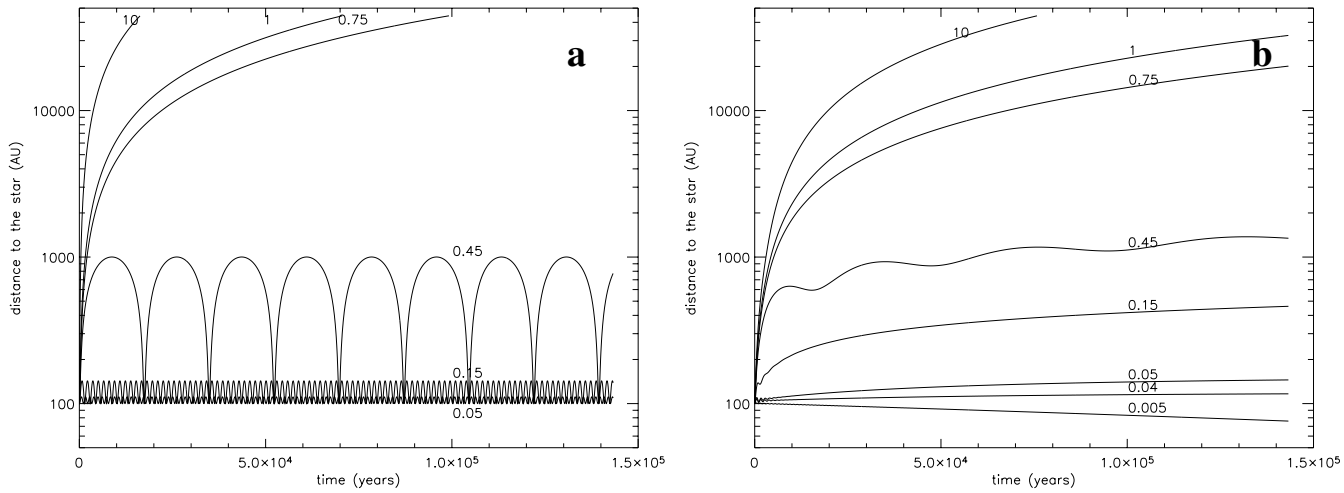

Fig. 2. Radial position as a function of time, for different values of β, for one particle initially located at 100 AU: **a)** gas-free case **b)** high gas density case (case 1). Note how efficient gas drag partially erases the abrupt transition at $\beta = 0.5$ for the dynamical behaviour of small grains.

as the "braking agent", maintaining all high β elements on Keplerian orbits.

We will also consider the case where the gas disc is truncated at 150 AU. Finally, an academic case where the gas distribution matches the classical Hayashi (1981) radial profile proportional to $r^{-2.75}$ is also tested. All initial conditions are summarized in Table 1.

2.4. Scattered light profile

The aim of the paper is to use the shape of the scattered light surface brightness profile along the disc midplane to set an upper limit on the gas density in the β Pictoris system. We detail in this section the procedure we used to calculate the brightness profile.

All particles are produced at an initial moment t_0 after which we let the system dynamically evolve. At *regular* time intervals we compute the brightness profile along the disc midplane assuming a perfectly edge-on disc. At each projected distance from the star and because the disc is assumed to be optically thin, the surface brightness is obtained by integrating the flux scattered by the dust particles along the line of sight. The stellar flux received by a grain is assumed to drop with the square of the distance from the star (stellar flux dilution in an optically thin environment). Scattering is assumed to be gray and isotropic. Gray scattering implies that the scattering cross section is proportional to the geometric cross section. For the isotropic assumption, see the discussion in Augereau et al. (2001) who showed that the anisotropic scattering properties of the grains only affect the regions below ≃80 AU as far as the scattered light radial brightness profile along the disc midplane is concerned. The final profile is progressively obtained by adding these instantaneous profiles. This procedure is stopped when no further significant evolution of the total profile is observed at projected distances smaller than 500 AU, either because particles eventually escape the system or are collisionally destroyed.

Our procedure is implicitly equivalent to assuming an arbitrarily constant dust production rate from parent bodies. The absolute value of the "real" production rate is here an unconstrained parameter that does not affect the results since we are only concerned with the shape of the surface brightness profile and not its absolute intensity. Thus, only the relative size distribution of the produced dust matters in our approach and not the exact amount of dust produced by collisions. Our results can be rescaled to any absolute flux level through the C_0 coefficient because the collisional lifetime of dust in the models has been scaled to the observed value rather than being dependent on the density of material in the disc.

3. Results

For sake of clarity, we will focus on three observational parameters, namely the two flux ratios in scattered light along

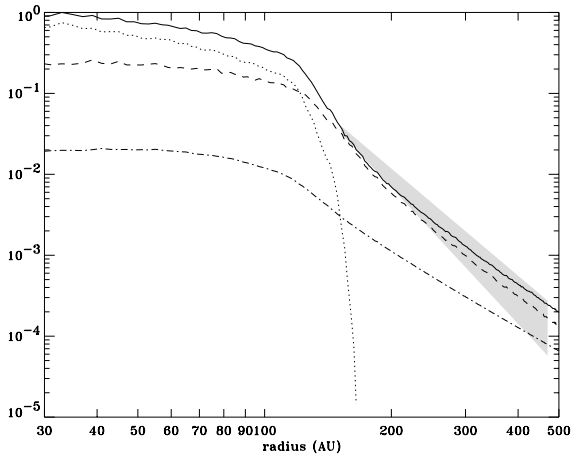

Fig. 3. Simulated scattered light mid-plane profile in a gas-free disc (solid line). The flux is arbitrarily rescaled so that its maximum value equals 1. The dotted line shows the contribution of the $0.005 < \beta < 0.05$ population, the dashed line that of the $0.05 < \beta < 0.5$ and the dash-dot line that of the $0.5 < \beta < 25$. The grey area shows the range of plausible profiles in the outer region, as deduced from Heap et al. (2000) observations for the SE and NW sides. It corresponds to the area bordered by $r^{-4.5}$ and $r^{-5.5}$ slopes derived from the flux value at 150 AU.

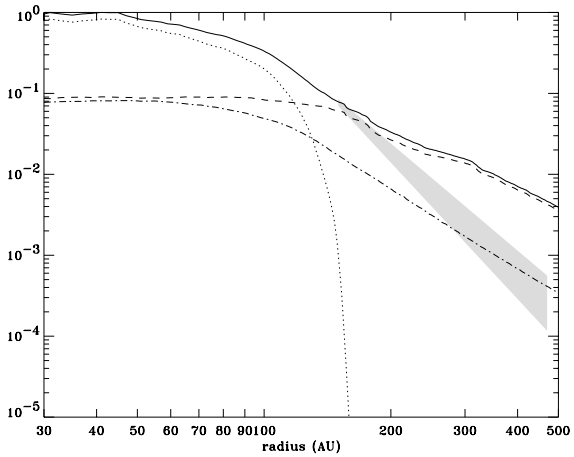

Fig. 4. Same as Fig. 3 but for the high gas density disc (case 1 in Table 1).

the disc midplane $F_{40/100} = F_{40\mathrm{AU}}/F_{100\mathrm{AU}}$ and $F_{400/100} = F_{400\mathrm{AU}}/F_{100\mathrm{AU}}$ and the averaged power law index p_{out} of the radial distribution profile measured between 150 and 400 AU. The reference observational values deduced from Heap et al. (2000) are $F_{40/100} \simeq 0.3$, $F_{400/100} \simeq 5 \times 10^{-3}$ (by extrapolating their profile) and $-5.5 < p_{\mathrm{out}} < -4.5$.

3.1. No gas

We first perform a test run with no gas drag in order to provide us with a reference case to which the following runs may be compared.

The synthetic scattered light profile displayed in Fig. 3 is close to the one obtained by Augereau et al. (2001), with $F_{40/100} \simeq 0.35$ and $F_{400/100} \simeq 5 \times 10^{-3}$. However, we find $p_{\mathrm{out}} \simeq -4.7$ while Augereau et al. (2001) obtain p_{out} between -5 and -5.5. This small difference has two causes. First, the presence of high β (>0.5) grains ignored in the dynamical approach of Augereau et al. (2001) moderately contributes to the flux in the outer regions (assuming a distribution of the $\beta > 0.5$ particles similar to those with $\beta \simeq 0.5$; Augereau et al. (2001) also found a similar trend). Second, we take into account here the collisional lifetime of the particles whereas Augereau et al. (2001) considered a phase mixing of randomly generated particle orbits. The dependence of t_{coll} on distance to the star tends to increase the density of the $\beta \simeq 0.5$ particles which spend a significant amount of time in the outer regions, hence the slightly flatter slope beyond 150 AU. However, this -4.7 slope is still in agreement with the radial power-law index measured by Heap et al. (2000) from the HST/STIS scattered light images: about -4.5 for the northeast side of the disc and about -5.5 for the southwest side. It should be noted that a slope index close to -5 for the scattered profile beyond the parent body region is in agreement with the results of Lecavelier et al. (1996) who proved this to be a natural tendency for such systems.

3.2. High gas density

In this section we consider the high gas density case, with $n_0 = 10^6$ cm^{-3} (case 1 in Table 1), as inferred by Thi et al. (2001) and as required by Brandeker et al. (2004) in order to have hydrogen act as a "braking agent" for observed high-β gaseous species.

Differences to the gas-free case remain negligible in the inner 100 AU region (Fig. 4), where the flux is dominated by the largest particles with $\beta < 0.05$ which are only moderately affected by gas drag (see Fig. 2). Furthermore, it should be noted that the limiting value β_{steady}, separating the regime where gaseous friction leads to inward drift ($\beta < \beta_{\mathrm{steady}}$) from the regime of outward drift ($\beta > \beta_{\mathrm{steady}}$), falls within this size-range (see Fig. 2b). Using Eqs. (27) and (28) of Takeuchi & Artymowicz (2001) with the present gas density, one gets $\beta_{\mathrm{steady}} = 0.034$.

In the $r > 150$ AU region, however, differences to the previous case are striking. The obtained brightness profile is clearly incompatible with the Heap et al. (2000) data, with $F_{400/100} \simeq 2 \times 10^{-2}$ and $p_{\mathrm{out}} \simeq -2.7$. This is mainly due to the strong increase of the $0.05 < \beta < 0.5$ particle contribution. This population is strongly affected by gaseous friction and is progressively driven into the outer disc, hence flattening the radial profile, whereas in the gas-free case only particles very close to the $\beta = 0.5$ limit have orbital eccentricities high enough to reach these regions (Fig. 2). This outward drift has the additional effect of lengthening the collisional lifetime of these particles (because of the radial dependency of the collision rate, cf. Eq. (6)). The contribution of the $\beta > 0.5$ particles is also increased with respect to the gas-free case. For these particles the effect of gas drag is on the contrary to slow down their radial escape, hence prolonging their stay in the disc (Fig. 2). Their contribution to the total flux nevertheless remains marginal.

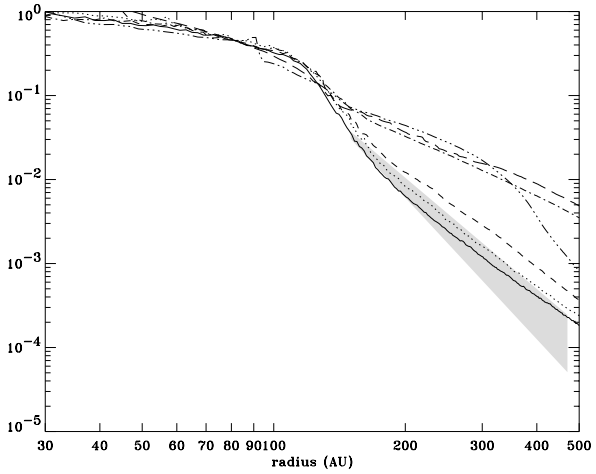

Fig. 5. Global profile for different gas disc prescriptions. Solid line: gas-free profile of Fig. 3. Then, from bottom to top of the profile values at 500 AU: Solar abundance reconstructed gas disc, i.e. Brandeker et al. (2004) profile with $n_0 = 2.25 \times 10^3$ cm^{-3}, same profile with $n_0 = 10^4$ cm^{-3}, Brandeker et al. (2004) profile with $n_0 = 10^6$ cm^{-3} truncated at 150 AU, Brandeker et al. (2004) profile with $n_0 = 10^5$ cm^{-3}, Hayashi profile with a total disc mass of 40 $M_\oplus$. These models correspond respectively to cases 2, 3, 5, 4 and 6 in Table 1.

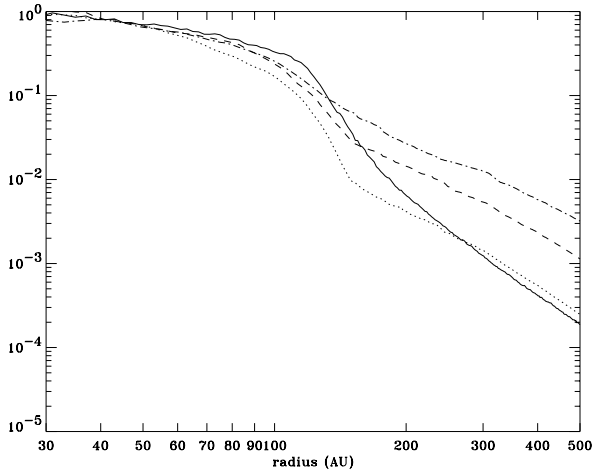

Fig. 6. Profiles obtained for different dust size distributions in the high gas density disc (case 1). dash-dot line: $dN \propto s^{-3.5}ds$, dashed line: $dN \propto s^{-3}ds$, dotted line: $dN \propto s^{-2.5}ds$. The solid line is the reference gas-free profile of Fig. 3.

It is one order of magnitude smaller than the flux produced by the $0.05 < \beta < 0.5$ particles between 100 and 400 AU (Fig. 4).

3.3. Exploring the gas density

Taking the low gas density distribution reconstructed by Brandeker et al. (2004) assuming solar abundances leads to a luminosity profile which is almost undistinguishable from the gas-free one (Fig. 5). Additional runs assuming the profile of Eq. (7) with varying n_0 show that departures from the gas-free case, and thus incompatibility with the observed Heap et al. (2000) luminosities, become significant for $n_0 > 10^4$ cm^{-3}. We also performed a test run with the high gas density distribution truncated beyond 150 AU. But this leads to a luminosity profile much too high around 150–300 AU, mainly because of the accumulation of the $0.05 < \beta < 0.5$ grains in this region. This accumulation is an effect already observed by Takeuchi & Artymowicz (2001) for small grains in truncated gaseous discs. An additional run with a total gas mass equal to that of case 2 (40 $M_\oplus$) but assuming a solar type profile in $r^{-2.75}$ (Hayashi 1981) also leads to strong departures from the observed luminosity profile in the outer region.

Note also that the dust luminosity profile in the inner 100 AU region is almost independent of gas drag effects, at least for the density range explored here.

3.4. Exploring the dust size distribution in the high gas density case

All luminosity profiles sofar were computed assuming that dust particles follow the classical $dN \propto s^{-3.5}ds$ size distribution, which is the prescription usually taken in similar studies (e.g. Augereau et al. 2001). However, it should be stressed that "real" size distributions may significantly depart from this theoretical collisional equilibrium power law, especially for particles close to the blow-out size (see Thébault et al. (2003) for a detailed discussion of this issue).

Accurately estimating the size distribution exceeds the scope of the present work, but we have tested alternative size-distribution power laws in order to explore how the final profile depends on this parameter. Figure 6 clearly shows that reducing the power-law index of the size distribution indeed leads to a drop of flux beyond 150 AU. However, the price to pay for this better fit in the outer disc is a significant and troublesome flux reduction in the 100–150 AU region. This leads to profiles that are as bad a fit to observational data as in the $dN \propto s^{-3.5}ds$ case. This flux reduction could in principle be compensated for by allowing the radial distribution of the parent bodies to extend further out. However, this would in turn lead to an increase of the flux beyond 150 AU, and thus departure from the good match originally obtained there, because the luminosity profile in these outer regions is mainly due to particles which originate from the highest parent body density region.

4. Discussion

The above results all tend to point towards an incompatibility between high gas densities and dust luminosity profiles matching observations. One could wonder however if these discrepancies may be eliminated by assuming parent body distributions that differ from that proposed by Augereau et al. (2001) in the context of a *gas-free* system. In this case the problem would become hopelessly degenerate: for each gaseous disc considered there would always be an ad-hoc parent body distribution producing a good fit to the observations.

We do not believe this to be the case because the simulations show that parent body distributions cannot be arbitrarily chosen either in the inner or in the outer regions of the disc. In the inner (<100 AU) region, the luminosity profile is dominated by large grains with $\beta < 0.05$ (see Fig. 4). These particles are

only weakly affected by gas drag and remain on nearly circular orbits matching those of the parent bodies producing them. It follows that, for the inner disc, a change of parent body distribution would automatically lead to departures from the best-fit luminosity profile which cannot be compensated by gaseous friction effects, at least within the gas density range explored in this paper (additional test runs have shown that significant departures from the gas-free profile are found in the inner disc when $n_0 > 10^7$ cm^{-3} which corresponds to unrealistically large amounts of gas).

Beyond 150 AU the problem becomes more complex and there might in principle be an alternative parent body distribution able to "bend" the outer disc profile towards the "correct" one even for the high gas density case. However, it is easy to see that in order to achieve this, this alternative distribution should act to *decrease* the outer disc luminosity by more than an order of magnitude (Fig. 4). This cannot be done by adjusting the parent body distribution in the outer disc, since in the reference case this distribution is already truncated beyond 150 AU, so any alternative distribution in the outer disc can only *add* objects there and result in an *increase* of the luminosity. Thus in order to lower the luminosity profile in the outer disc the only possibility is to change the parent body distribution in the *inner* disc. But, as has just been shown, this cannot be done without in turn strongly modifying the luminosity profile in the inner regions (which would result in departing from a good fit of observations), thus solving one problem by creating another. As a consequence, we do believe the Augereau et al. (2001) parent body profile to be a rather robust assumption.

Alternatively, one may consider different dust size distributions, for instance a shallower distribution in order to lower the flux in the outer regions where small grains dominate. However, Fig. 6 shows that this does not work either. We cannot completely exclude the possibility that a fine-tuned fit might be found by letting the size distribution depend on the distance to the star and find an ad-hoc adjustment at all distances, but such a thorough parameter exploration is beyond the scope of the present work. However, even if such an ad-hoc fit could be found, it would have the disadvantage of being less generic.

Another parameter space that was left unexplored here is the grain scattering properties. However, for dust radial distributions relatively similar to the present ones, Augereau et al. (2001) have shown that assuming anisotropic scattering properties for the grains would not significantly affect the flux profile beyond ~80 AU, i.e. the region of interest for the present discussion.

Under these assumptions we thus believe that the present simulations rule out the presence of large amounts of gas around β Pictoris, especially in the outer parts of the disc. Assuming the profile of Brandeker et al. (2004), the upper limit on the n_0 value is $\simeq 10^4$ cm^{-3} corresponding to a total gas mass of $\simeq 0.4\ M_\oplus$. This corresponds to a gas to dust ratio smaller or approximatively equal to 1 at most.

5. Summary and conclusion

We have numerically investigated the dynamics of dust particles suffering a gas drag force in the edge-on β Pictoris disc. From our simulations we were able to compare theoretical scattered light profiles along the disc midplane to the reference images obtained by Heap et al. (2000). Several gas disc prescriptions and a broad range of grain sizes (from $\beta = 0.005$ to $\beta = 25$) have been explored. We assumed that dust particles are produced by parent bodies following the distribution derived by Augereau et al. (2001), an assumptiom which our simulations prove to be relatively robust.

Our main result is that high density gas discs always lead to dust distributions whose luminosity profiles are strongly incompatible with the observations in the outer regions of the disc (beyond 150 AU), while the surface brightness profile in the inner regions is poorly sensitive to the effect of gas drag on the grains. Assuming the gas density profile of Brandeker et al. (2004), gas discs with total mass above ~0.4 $M_\oplus$ seem to be ruled out. This value is consistent with the H_2 upper limit obtained by Lecavelier et al. (2001) and with the total gas mass estimated by Kamp et al. (2003). It is also consistent with the gas mass upper limit found by Chen et al. (2004) based on recent Spitzer mid-infrared observations. Unless the gas disc is surprisingly very extended so that the dust dynamics is not affected by gas drag within the first hundreds of AU from the star, our results tend to rule out the much higher gas mass estimate (50 $M_\oplus$) derived by Thi et al. (2001). However, this leaves open the puzzling problem of high β ions observed on bound orbits, since it also rules out the gaseous braking agent hypothesis for which at least 40 $M_\oplus$ of hydrogen are required according to Brandeker et al. (2004). Our results suggest that other scenarios, like braking by other chemical species or by a magnetic field, should be investigated. This may lead to a better estimate of the mass of gaseous species insensitive to stellar radiation pressure required to stop high β ions (Beust & Valiron 2005). The approach developed in the present paper could also be applied to similar debris disc systems, in particular the recently discovered disc around AU Mic, which is coeval with β Pictoris (Kalas et al. 2004).

Acknowledgements. The authors thank C. Chen and K. Stapelfeldt for providing information regarding the interpretation of their Spitzer observations of β Pictoris. This work is supported by the European Research Training Network "The Origin of Planetary Systems" (PLANETS, contract number HPRN-CT-2002-00308).

References

Artymowicz, P. 1988, ApJ, 335, L79
Artymowicz, P. 1997, Ann. Rev. Earth Planet. Sci., 25, 175
Augereau, J. C., Nelson, R. P., Lagrange, A. M., Papaloizou, J. C. B., & Mouillet, D. 2001, A&A, 370, 447
Beust, H., & Valiron, P. 2005, A&A, in preparation
Brandeker, A., Liseau, R. G., & Fridlund, M. 2004, A&A, 413, 681
Chen, C. H., Van Cleve, J. E., Watson, D. M., et al. 2004, Am. Astron. Soc. Meet. Abstr., 204, #41.06
Dent, W. R. F., Walker, H. J., Holland, W. S., & Greaves, J. S. 2000, MNRAS, 314, 702
Deller, A. T., & Maddison, S. T. 2005, ApJ, in press
Di Folco, E., Thévenin, F., Kervella, P., et al. 2004, A&A, 426, 601
Dohnanyi, J. S. 1969, JGR, 74, 2531
Freudling, W., Lagrange, A.-M., Vidal-Madjar, A., Ferlet, R., & Forveille, T. 1995, A&A, 301, 231

Hayashi, C. 1981, PthPS, 70, 35
Heap, S. R., Lindler, D. J., Lanz, T. M., et al. 2000, ApJ, 539, 435
Hobbs, L. M., Vidal-Madjar, A., Ferlet, R., Albert, R. C., & Gry, C. 1985, ApJ, 293, L29
Kalas, P., & Jewitt, D. 1995, AJ, 110, 794
Kalas, P., Liu, M. C., & Matthews, B. C. 2004, Science, 303, 1990
Kamp, I., van Zadelhoff, G.-J., van Dishoeck, E. F., & Stark, R. 2003, A&A, 397, 1129
Kwok, S. 1975, ApJ, 198, 583
Lagrange, A.-M., Beust, H., Mouillet, D., et al. 1998, A&A, 330, 1091
Lecavelier des Etangs, A., Vidal-Madjar, A., & Ferlet, R. 1996, A&A, 307, 542
Lecavelier Des Etangs, A., Vidal-Madjar, A., & Ferlet, R. 1998, A&A, 339, 477
Lecavelier des Etangs, A., Vidal-Madjar, A., Roberge, A., et al. 2001, Nature, 412, 706
Liseau, R., White, G. J., Larsson, B., et al. 1999, A&A, 344, 342
Liseau, R. 2003, ESA Special Publication, SP-539, 135
Okamoto, Y. K., Kataza, H., Honda, M., et al. 2004, Nature, 431, 660
Olofsson, G., Liseau, R., & Brandeker, A. 2001, ApJ, 563, L77
Pantin, E., Lagage, P. O., & Artymowicz, P. 1997, A&A, 327, 1123
Roberge, A., Feldman, P. D., Lagrange, A. M., et al. 2000, ApJ, 538, 904
Smith, B., & Terrile, R. 1984, Sci, 226, 1421
Song, I., Zuckerman, B., & Bessel, M. S. 2003, ApJ, 599, 342
Takeuchi, T., & Artymowicz, P. 2001, ApJ, 557, 990
Telesco, C. M., Fisher, R. S., Wyatt, M. C., et al. 2005, Nature, 433, 133
Thébault, P., Augereau, J.-C., & Beust, H. 2003, A&A, 408, 775
Thi, W. F., Blake, G. A., van Dishoek, E. F., et al. 2001, Nature, 409, 60
Vidal-Madjar, A., Lagrange-Henri, A.-M., Feldman, P. D., et al. 1994, A&A, 290, 245
Wyatt, M. C., & Dent, W. R. F. 2002, MNRAS, 334, 589
Zuckerman, B., & Becklin, E. E. 1993, ApJ, 414, 793
Zuckerman, B., Song, I., Bessel, M. S., & Webb, R. A. 2001, ApJ, 562, L87